Available online at www.sciencedirect.com
SCIENCE DIRECT®
International Journal of Mass Spectrometry 228 (2003) 389–402
International Journal of Mass Spectrometry
www.elsevier.com/locate/ijms

How ergodic is the fragmentation of the pyridine cation? A maximum entropy analysis

E. Gridelet, R. Locht, A.J. Lorquet, J.C. Lorquet[1], B. Leyh[*,2]

Department of Chemistry, University of Liège, B. 4000 Sart Tilman, Belgium

Received 14 November 2002; accepted 18 March 2003

Abstract

The kinetic energy released to the $C_4H_4^+$ and HCN fragments produced by the dissociation of the pyridine ion has been determined by a retarding field technique up to an internal energy of 4 eV above the reaction threshold. This extends our previous study limited to the metastable domain [Int. J. Mass Spectrom. Ion Process. 185/186/187 (1999) 155]. Retarding potential curves resulting from dissociative photoionization using the He(I), Ne(I), and Ar(II) resonance lines have been analyzed by the maximum entropy method. The comparison between the experimentally measured curves and those calculated for the prior (i.e., most statistical) situation reveals the existence of dynamical constraints that prevent phase space from being fully explored. The "ergodicity index" $F(E)$ that measures the efficiency of phase space sampling as a function of the internal energy E of the molecular ion is found to decrease steadily as a function of E and to level off at a value of about 50% when $E \geq 2.5$ eV. At these high internal energies where phase space exploration no longer decreases, spontaneous intramolecular vibrational energy redistribution (i.e., resulting from the anharmonicity of the molecular vibrations) is thought to contribute to internal energy randomization to a limited extent only. When the lifetime is short, phase space exploration is believed to result instead from the relaxation of the electronic energy via a cascade of non-radiative transitions, which leads to a great diversity of initial conditions, and thus, contributes to statisticity.

Keywords: Kinetic energy release; Maximum entropy method; Phase space; Pyridine ion; $C_4H_4^+$ ion; Statistical theory

1. Introduction

All statistical theories of mass spectra assume fast randomization of the internal energy before dissociation takes place. A molecule is said to behave ergodically if reactive nuclear trajectories sample the available part of phase space either fully or at least representatively before dissociation [1–4].

In 1981, Professors Helmut Schwarz and Chava Lifshitz started to investigate evidence for non-ergodic behavior in ionic fragmentations [5] and pointed out that the analysis of the translational energy distribution carried by the fragments of a unimolecular dissociation gives information about the ergodic nature of the reaction [3]. The present article wishes to follow

* Corresponding author. Tel.: +32-4-366-3425; fax: +32-4-366-3413.
E-mail addresses: Evelyne.Gridelet@ulg.ac.be (E. Gridelet), Robert.Locht@ulg.ac.be (R. Locht), alorquet@ulg.ac.be (A.J. Lorquet), JC.Lorquet@ulg.ac.be (J.C. Lorquet), Bernard.Leyh@ulg.ac.be (B. Leyh).
[1] Co-corresponding author. Fax: +32-4-366-3413.
[2] Research associate of the F.N.R.S., Belgium.

1387-3806/$ – see front matter © 2003 Elsevier Science B.V. All rights reserved.
doi:10.1016/S1387-3806(03)00132-5

up this idea. A key concept studied in the Schwarz group, namely the seam between crossing potential energy surfaces [6–8], will be suggested to provide an important clue to the problem. Our paper is dedicated to Helmut, in recognition of his lifelong insistence that theory and experiment should always work in concert.

The present contribution exploits a definition of the degree of ergodicity provided by the maximum entropy theory [9–12]. This method has been previously applied to simple reactions, consisting mainly in a straightforward bond cleavage leading to the loss of a halogen neutral atom [13–15]. We now turn to a more complicated reaction:

$$C_5H_5N^+ \rightarrow C_4H_4{}^+ + HCN \quad (1)$$

This reaction is interesting and challenging for several reasons. First, it is one of the benchmark reactions that have been studied in the micro- and millisecond time scales and whose rate constant is known as a function of internal energy [16–19]. Second, this reaction requires an important reorganization of the molecular structure. An aromatic six-membered ring generates a $C_4H_4{}^+$ fragment whose most stable structure is that of the methylenecyclopropene [18–27]. Third, since the HCN fragment is characterized by a substantial dipole moment, the last step of the reaction is governed by a strongly anisotropic potential, in contradistinction to the reactions previously studied, which involved asymptotically isotropic long-range forces. Fourth, from an experimental point of view, the thermal energy is not negligibly small with respect to the translational energy release, so that a new method had to be developed to extract the kinetic energy release distribution from the raw data.

The question we investigate in the present article is "to what extent is reaction (1) ergodic?". An answer to that question has already been provided when the internal energy is such that the reaction takes place in the microsecond time scale [28]. However, in the present paper, we wish to extend the analysis to a substantially broader range of internal energies.

2. Experimental technique and data handling

2.1. Apparatus and experimental working conditions

The spectrometer is constituted by a Lindau-type electron energy analyzer and an ion retarding potential device coupled with a quadrupole mass analyzer [29,30]. Fig. 1 shows the ionization chamber together with the ion optics necessary to perform retarding field experiments. The effusive gas sample is ionized by photons produced by a rare gas discharge lamp, along a direction perpendicular to the figure plane. He(I) (21.21 eV), Ne(I) (16.65–16.87 eV) and Ar(II) (13.47 eV) resonance lines were used in the present contribution. The device is surrounded by a mu-metal cylinder, protecting against residual magnetic fields.

The ions are retarded within the chamber by applying a variable voltage to the EXE lens (see Fig. 1), while the ion chamber and the EXI extractor are kept at constant potential. Ions are focused to the entrance slit of the quadrupole mass spectrometer by two triplet lenses (L1 to L4) and by an intermediate F lens.

The transmission of the ion optics-quadrupole system has been checked carefully. In the ion energy range of interest, and well above (up to 4 eV), the transmission is constant within maximum limits of ±10%.

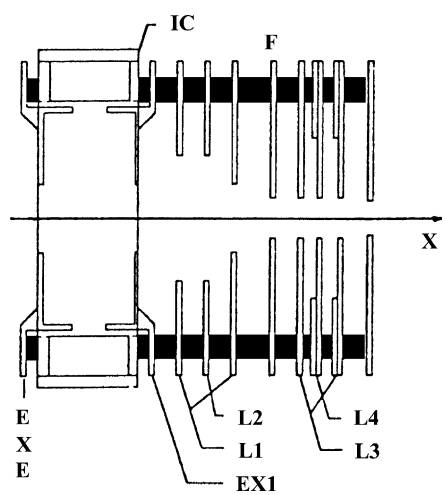

Fig. 1. Schematic view of the ionisation chamber and ion optics.

Pyridine (HPLC grade, 99.9% purity) and pyridine-d_5 (100% atom purity) from Aldrich were used without further purification. The retarding potential curves of both the ionic fragment ($C_4H_4^+$) of interest and the parent ion ($C_5H_5N^+$) were recorded sequentially.

2.2. Data handling

What we are interested in is the kinetic energy release distribution (KERD) of the pair of fragments, i.e., the distribution of their relative translational energy when they fly apart in the three-dimensional space. The total translational energy released, ε, is shared among both fragments according to the conservation of linear momentum, so that the translational energy of the ionic fragment is $\varepsilon_f = \varepsilon(m_n/(m_n+m_f))$, where m_f and m_n are, respectively, the masses of the ionic ($C_4H_4^+$) and neutral (HCN) fragments. Besides, the experimental device strongly discriminates in favor of the x direction (i.e., the optical axis of the spectrometer), so that the KERD, noted $\tilde{P}(\varepsilon_f)$ or $\tilde{P}(\varepsilon)$, cannot be directly equated to the derivative of the ion retarding curve, $I(\varepsilon_f)$. However, ion trajectory simulations have shown that the KERD can be related to $I(\varepsilon_f)$ by a simple empirical relationship [31]:

$$\tilde{P}(\varepsilon_f) \propto \varepsilon_f^{\mu} \frac{dI(\varepsilon_f)}{d\varepsilon_f} \tag{2}$$

where $\mu = 0.43 \pm 0.03$. The kinetic energy release ε_f is simply the product of the retarding potential by the charge of the ion. The ε_f^{μ} factor corrects for the discrimination effects.

Eq. (2) is valid when the average kinetic energy that is delivered to the fragment ion upon dissociation strongly exceeds the thermal energy of the parent ion. If this is not the case, a deconvolution procedure must be applied, as now explained.The velocity of the fragment ion ($\vec{v}_f$) is the vectorial sum of the initial velocity of the parent ion ($\vec{v}_p$) and of the velocity component ($\vec{v}_d$) associated with the release of translational energy upon dissociation:

$$\vec{v}_f = \vec{v}_p + \vec{v}_d \tag{3}$$

The three-dimensional velocity distribution can then be written as a convolution product:

$$\tilde{P}(\vec{v}_f) = \tilde{P}(\vec{v}_p)\tilde{P}(\vec{v}_d) \tag{4}$$

To solve this deconvolution problem, we first assume that both velocity distributions $\tilde{P}(\vec{v}_p)$ and $\tilde{P}(\vec{v}_d)$ are isotropic, so that a simple equation relates the velocity distributions to the associated kinetic energy distributions. For the fragment ion, we can write $\tilde{P}(\varepsilon_f)\,d\varepsilon_f = \tilde{P}(v_f)\,dv_f$, where $v_f = |\vec{v}_f| = \sqrt{2\varepsilon_f/m_f}$, and, integrating over angular coordinates:

$$\tilde{P}(\varepsilon_f)\,d\varepsilon_f = 4\pi v_f^2 \tilde{P}(\vec{v}_f)\,dv_f \tag{5}$$

A similar equation holds for the parent ion.

The velocity distribution for the parent ion can be considered as a Maxwell distribution determined by the ion source temperature. One possible procedure would now consist in extracting the isotropic distribution $\tilde{P}(\vec{v}_f)$ from the experimental retarding potential curve by using Eq. (2) together with Eq. (5). And then, in a second step, deconvolution via Eq. (4) leads to $\tilde{P}(\vec{v}_d)$, from which a KERD free from the thermal energy contribution could be deduced using again Eq. (5). However, the use of Eq. (2) implies a numerical differentiation, with a concomitant increase of the noise level of the experimental data, making the deconvolution procedure quite hazardous. We decided, therefore, to work directly on the ion retarding curve, $I(\varepsilon_f)$. Inserting Eq. (5) into Eq. (2) leads to

$$\begin{aligned} I(\varepsilon_f) &\propto \int \varepsilon_f^{-\mu}[v_f(\varepsilon_f)]^2 \frac{dv_f(\varepsilon_f)}{d\varepsilon_f} \tilde{P}[\vec{v}_f(\varepsilon_f)]\,d\varepsilon_f \\ &\propto \int \varepsilon_f^{-\mu}\varepsilon_f^{0.5}\tilde{P}[\vec{v}_f(\varepsilon_f)]\,d\varepsilon_f \end{aligned} \tag{6}$$

The following procedure is now adopted:

(i) The parent ion velocity distribution is assumed to correspond to Maxwell equation:

$$\tilde{P}(\vec{v}_p)\,d\vec{v}_p = A\exp(-\alpha v_p^2)\,dv_{p,x}dv_{p,y}dv_{p,z} \tag{7}$$

where A is a normalization coefficient and α is obtained by fitting the parent ion signal.

(ii) The velocity distribution $\tilde{P}(\vec{v}_d)$ is calculated, using Eq. (5), with an appropriate Ansatz for the

corresponding kinetic energy release distribution. From our previous work in the metastable domain [28], we expect a monotonous Maxwell–Boltzmann-like distribution. This is also suggested by the structureless behavior of the retarding potential curves in the present photodissociation experiments. As will be shown below, the analytical form predicted by the maximum entropy method (see Section 3.2, Eq. (13)), which depends on Lagrange parameters, is an appropriate Ansatz for the present distributions. Anticipating on Section 3, we already give the appropriate analytical form of the KERD, for a given internal energy, E, of the parent ion:

$$P(\varepsilon|E) = P^0(\varepsilon|E)\exp[-\lambda_0(E) - \lambda_1(E)\varepsilon^k] \quad (8)$$

$P(\varepsilon|E)$ is the probability to release a translational energy ε to the fragments if the internal energy of the parent ion is equal to E. $P^0(\varepsilon|E)$ is the so-called prior, i.e., most statistical distribution, discussed in Section 3.1. λ_0 and λ_1 are internal energy dependent Lagrange parameters and ε^k is a constraint governing the energy transfers along the reaction coordinate during the dissociation process (more on this in Section 3.2). The distribution given by Eq. (8) has to be averaged over the internal energy distribution, $T(E)$ of the parent ion (as explained in Section 5, Eq. (18)).

(iii) The Maxwell distribution and the velocity distribution derived from the maximum entropy formalism are then convoluted analytically (Eq. (4)). The resulting distribution is introduced into Eq. (6), leading to Eq. (9), which takes the average over $T(E)$ into account:

$$I(\varepsilon_f) = A' \int \mathrm{d}\varepsilon_f\, \varepsilon_f^{-\mu} \exp\left(\frac{-2\alpha\varepsilon_f}{m_f}\right) \times \int_0^{+\infty} \mathrm{d}x \exp\left(\frac{-2\alpha x}{m_f}\right) \sinh\left(\frac{4\alpha\sqrt{\varepsilon_f x}}{m_f}\right) \times \int_{\varepsilon(x)}^{+\infty} \mathrm{d}E\, T(E)\, P^0(x|E) \exp[-\lambda_0(E) - \lambda_1(E)x^k] \quad (9)$$

where A' is a normalization coefficient.

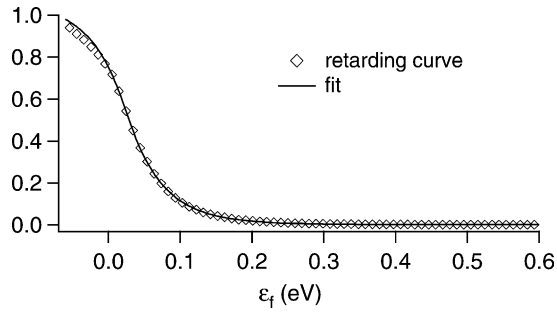

Fig. 2. A typical retarding curve and its fit to Eq. (9) with $k = 1/2$. The diamonds stand for the experimental curve and the solid line stands for the fit using Eq. (9). Note that the fit actually begins at $\varepsilon_f = -0.001$ eV. For the clarity of the figure, the diamonds give only one out of four experimental points.

(iv) Eq. (9) is then fitted by non-linear least square analysis to the experimental retarding curve, providing us with the best-fit Lagrange multipliers, which are the basic ingredients of the maximum entropy method. Fig. 2 displays a typical retarding curve fitted to Eq. (9). Note that exponent k is also a parameter but it is kept fixed in the fitting procedure. Several values of k are then tested sequentially (more on this in Section 5). The excellent agreement between the fit and the experimental data shows that the maximum entropy Ansatz is appropriate for the present experimental situation. It has been checked that the experimental uncertainty on the empirical μ exponent has no significant influence on the parameters derived from the fit.

3. Maximum entropy formalism: a summary

We now show that the maximum entropy method can provide an answer to our original question: To what extent is the lowest-energy fragmentation of the pyridine cation ergodic?

3.1. The prior distribution

First of all, one has to look for a criterion for non-ergodicity. Consider a situation where the internal

energy is totally randomized in the parent ion, i.e., where the reactive nuclear trajectories visit all parts of phase space before reacting. Then phase space is sampled in an ergodic way and all the quantum states of the system are equally probable. In this ideal situation, the probability to release an amount of translational energy ε if the internal energy is equal to E is termed the prior distribution and is denoted $P^0(\varepsilon|E)$. By its very definition, it is proportional to the density of states [1,9–12]:

$$P^0(\varepsilon|E) \propto \varepsilon^{1/2} N_{\text{int}}(E-\varepsilon) \tag{10}$$

where $\varepsilon^{1/2}$ is proportional to the density of states of the three-dimensional relative translational motion of the centers of mass of the two fragments and $N_{\text{int}}(E-\varepsilon)$ denotes their internal (vibrotational) density of states. The prior distribution is normalized, i.e.,

$$\int_0^E P^0(\varepsilon|E)\,\mathrm{d}\varepsilon = 1 \tag{11}$$

If the experimental distribution $P(\varepsilon|E)$ differs from $P^0(\varepsilon|E)$, it can be suspected that the reaction is not totally ergodic. One or several dynamical constraints can be anticipated to introduce a bias in the exploration of phase space, favoring some quantum states at the expense of others. The most obvious constraints are the conservation of energy and angular momentum. Eq. (10) ensures that conservation of energy is included in the prior distribution, in contradistinction to the conservation of angular momentum. The role of the latter is currently under study. However, the maximum entropy formalism makes it possible to identify constraints that could be less widely known than the two ones that we have just mentioned. This question will be discussed in Section 3.2.

3.2. The reaction constraints

In the maximum entropy method, the actual KERD $P(\varepsilon|E)$ is related to the prior distribution by the following equation [9–12]:

$$P(\varepsilon|E) = P^0(\varepsilon|E)\exp[-\lambda_0(E)]\exp[-\lambda_1(E)\varepsilon^{k_1}] \times \exp[-\lambda_2(E)\varepsilon^{k_2}]\cdots \tag{12}$$

where k_1, k_2, k_3, are rational numbers. The quantities $\lambda_i(E)$ are energy-dependent Lagrange multipliers. The quantities ε^{k_i} are termed the constraints (or the informative variables). It has been demonstrated [32] that if the exponents k_i as well as the functions $\lambda_i(E)$ are correctly chosen, and if the number of factors $\exp[-\lambda_i(E)\varepsilon^{k_i}]$ is large enough, then the right-hand-side of Eq. (12) converges to an exact quantum–mechanical result for $P(\varepsilon|E)$. However, the power of the method results from the fact that, in many instances, it is not really necessary to introduce a large number of factors into Eq. (12). In practice, the very simple expression

$$P(\varepsilon|E) = P^0(\varepsilon|E)\exp[-\lambda_0(E)]\exp[-\lambda_1(E)\varepsilon^{k}] \tag{13}$$

is found to provide already a very good approximation to $P(\varepsilon|E)$ if the value of the exponent k is adequately chosen. At least two reasons can be given for this unexpected simplification in the present experimental situation. First, the measured retarding curve to be analyzed has a simple shape, without any fine structure. Second, the present experiment involves extensive averaging over a large energy range. Note that the function $\lambda_0(E)$ is determined by the condition that the KERD be normalized at each energy E:

$$1 = \int_0^E P(\varepsilon|E)\,\mathrm{d}\varepsilon = \exp[-\lambda_0(E)] \times \int_0^E P^0(\varepsilon|E)\exp[-\lambda_1(E)\varepsilon^{k}]\,\mathrm{d}\varepsilon \tag{14}$$

3.3. The entropy deficiency DS and the ergodicity index F(E)

In information theory, the entropy measures the missing information. The higher the entropy, the greater the uncertainty about the state of the system. (Recall that an entropy equal to zero means that the state is completely determined.) This can be done, both for the prior distribution $P^0(\varepsilon|E)$ (giving the result S^0) and for the actual KERD $P(\varepsilon|E)$ (giving the result S).

The quantity $DS = S^0 - S$, termed the entropy deficiency, is always positive [9–12]. A non-zero entropy deficiency indicates a lack of energy randomization during the entire reactive process. It can be demonstrated that

$$DS(E) = S^0 - S = \int_0^E P(\varepsilon|E) \ln\left[\frac{P(\varepsilon|E)}{P^0(\varepsilon|E)}\right] d\varepsilon$$

can also be written

$$DS(E) = -\lambda_0(E) - \lambda_1(E)\langle\varepsilon^k\rangle(E) \quad (15)$$

where the averaged constraint $\langle\varepsilon^k\rangle(E)$ is given by

$$\langle\varepsilon^k\rangle(E) = \int_0^E \varepsilon^k P(\varepsilon|E)\, d\varepsilon \quad (16)$$

For example, when $k = 1$, $\langle\varepsilon\rangle(E)$ represents the average translational energy release, defined as the first moment of an internal energy selected KERD.

It can be demonstrated [11,33] that the quantity $\exp[-DS(E)]$ represents the ratio between the volume of phase space effectively explored during the reaction and the volume of phase space available to it at the internal energy E. Therefore, an ergodicity index:

$$F(E) = \exp[-DS(E)] \quad (17)$$

can be defined to measure the efficiency of phase space sampling as a function of the internal energy. The main purpose of the present work is to determine this function.

4. Computation of the prior distribution

4.1. Structure of the $C_4H_4^+$ fragment

As shown in Eq. (10), the calculation of the prior distribution requires the evaluation of the vibrotational density of states of the fragments as a function of the internal energy. The HCN fragment has the hydrogen cyanide structure [34–36]. Several low-energy isomeric forms of $C_4H_4^+$, however, coexist and could be produced upon dissociation of the pyridine cation. Early studies of the metastable dissociation of $C_5H_5N^+$ [18,19,21–23] based on appearance energy measurements, ion–molecule reactions and collisional activation, led to the conclusion that the $C_4H_4^+$ fragment produced at low internal energy has a low enthalpy of formation ($\Delta_f H = 1177\,kJ\,mol^{-1}$), and must therefore, correspond to either a single cyclic structure or to a mixture of two structures, one of them being cyclic. The methylenecyclopropene as well as the cyclobutadiene structures have been suggested. At higher internal energies, a mixture of two isomers has been pointed out [22]. Photoelectron spectroscopy of methylenecyclopropene leads to the determination of the enthalpy of formation of its cation ($\Delta_f H = 1178\,kJ\,mol^{-1}$) [24]. Together with CAD measurements on $C_4H_4^+$ resulting from direct ionization of methylenecyclopropene, this argument provides strong evidence that the cyclic structure formed at low internal energy is that of methylenecyclopropene. New activation techniques were developed in the late eighties, in particular neutralization–reionization mass spectrometry (NRMS), as diagnostic tools for the structure of ions and neutrals. The isomeric $C_4H_4^+$ cations vinylacetylene, butatriene, methylenecyclopropene and cyclobutadiene were investigated by the group of McLafferty and coworkers [37] and this information was later used to perform mixture analysis for various dissociations leading to $C_4H_4^+$ [38], unfortunately not that of the pyridine cation. Ion–molecule reactions of the same four $C_4H_4^+$ isomers were investigated by Shay et al. [39]. More recently, Koster and van der Hart [40] explored the photoinduced isomerization of $C_4H_4^+$ and concluded that the barrier connecting ionized vinylacetylene to the methylenecyclopropene structure lies below its dissociation limit. On the whole, it is now generally accepted that the $C_4H_4^+$ cations generated by the fragmentation of a wide variety of precursor ions are a mixture of cations having the methylenecyclopropene structure (~68% if the precursor is the benzene ion [38]) or the vinylacetylene ion structure (~32% if the precursor is $C_6H_6^+$ [38]). Unfortunately, the yields for reaction (1) have not been determined.

Several ab initio calculations, carried out by different authors, are available in the literature [25–27]. For our part, we studied the stable isomers with the B3LYP

density functional and QCISD methods using different basis sets, up to Dunning's correlation-consistent triple-dzeta basis set. (The significance of standard quantum–chemical acronyms is explained in many textbooks, e.g., [41].) A search for transition states was also attempted with the low-cost B3LYP/6-31G(d) method and intrinsic reaction coordinate calculations were then carried out to ascertain the interconnections between isomers. However, we could not detect any other saddle points than those previously studied by Hrouda et al. [25] and by Koster and van der Hart [27] with methods more elaborate than DFT. To summarize all available results, the calculations unanimously predict the existence of four low-lying isomers of the $C_4H_4^+$ ion of comparable energies, separated by potential barriers found in all the calculations to be as high as 2.2 eV or more. The most stable $C_4H_4^+$ isomer has the methylenecyclopropene structure. The other isomers are the cations of vinylacetylene, butatriene, and cyclobutadiene. The cyclobutadiene cation exists in two different forms, denoted rectangular or rhombic, but this is of no importance in the problem at hand. The most reliable results in our opinion are given in Table 1. It is particularly gratifying to note that three different methods to take into account the electronic correlation generated energy values that are in nearly quantitative agreement with one another. More details on the potential energy surface are given in refs. [25,27]. We recommend the use of the values calculated by Hrouda et al. [25] using the coupled-cluster method with a correlation-consistent triple-dzeta basis set (second column of Table 1).

Table 1
Energies (in eV) calculated for the stable isomers and transition states of the $C_4H_4^+$ ion measured with respect to the most stable conformation

	Method		
	CCSD(T)/cc-pVTZ//QCISD/6-31G(d)	MRCI//ROHF/6-31G(d,p)	QCISD/cc-pVTZ//QCISD/cc-pVDZ
	Reference		
	[25]	[27]	This work
	Size of AO basis set		
	176	80	176
MCP	0	0	0
VA	0.43	0.48	0.47
BT	0.32	0.26	0.39
CB	0.32	0.39	0.40
TVA	2.35	2.52	
TBT	2.19	2.47	
TCB	2.70	3.17	

MCP = methylenecyclopropene; VA = vinylacetylene; BT = butatriene; CB = cyclobutadiene. TVA, TBT, and TCB denote the height of the barrier which separates the isomers VA, BT, and CB, respectively, from the most stable isomer MCP.

4.2. Calculation of the prior distribution

The vibrational frequencies and rotational constants of the four low-lying isomers, as well as those of the corresponding perdeuterated species were calculated at the B3LYP/6-31G(d) level of theory recommended by Scott and Radom for that purpose [42]. The densities of states of the different species were then calculated by a Beyer–Swinehart state-counting algorithm [1,2] and substituted into Eq. (10) to determine the corresponding prior distributions.

The densities of states $N_{\text{int}}(E)$ of the two most likely isomers of the $C_4H_4^+$ fragment ion (i.e., methylenecyclopropene and vinylacetylene) were found to increase at the same rate and their ratio was observed to remain nearly constant over the entire energy range from 0 to 8 eV. The same is true for the butatriene cation. It can, therefore, be concluded that the prior distribution is independent of the nature and relative amount of the isomers generated in the photodissociation. In other words, the possible simultaneous production of these isomers in an unknown ratio has in this case no influence on the maximum entropy analysis of the problem, and can therefore, be ignored.

However, conservation of angular momentum is not introduced in the derivation of the prior distribution for the following reason. The constraints resulting from the conservation theorems might only be taken into consideration in a secure way when the potential between separating fragments is central (as in the ion-induced dipole interaction) over a substantial part of reaction path and, even then, at great pains.

This is not the case for the present reaction, which involves the loss of a HCN fragment characterized by a substantial dipole moment. We therefore preferred to choose a reliable starting point by including only the conservation of energy. As a consequence, part of the entropy deficiency deduced from our analysis could be due to the constraint of the conservation of angular momentum.

5. The distribution of internal energy *T(E)*

In principle, the course to be adopted in a maximum entropy analysis is as follows. The prior distribution is determined from ab initio calculations. The exponent k involved in the constraint ε^k is given a fixed value (i.e., either $k = 0.5$, or 1, or 2, from past experience). The numerical treatment then aims at determining the unknown function $\lambda_1(E)$ by fitting Eq. (13) to the experimentally determined KERD $P(\varepsilon|E)$. The function $\lambda_0(E)$ is determined via Eq. (14). The calculation of the entropy deficiency DS and of the ergodicity index $F(E)$ follows from Eqs. (15) to (17).

However, our experimental set-up does not generate energy-resolved measurements, because the parent ions $C_5H_5N^+$ are created by photoionization at fixed wavelength. They are characterized by a distribution of internal energies that is given by the photoelectron spectrum of pyridine. In addition, not all of the $C_5H_5N^+$ ions dissociate via reaction (1) (whose threshold is located 11.95 eV above the ground state of the neutral pyridine [18]), because other dissociation channels may be open if the internal energy is high enough. Therefore, the KERD $\tilde{P}(\varepsilon)$ that has to be considered in the present experiment is given by an average over a distribution function $T(E)$ that is equal to the product of the photoelectron spectrum and the appropriate branching ratio:

$$\begin{aligned}\tilde{P}(E) &= \int_{\varepsilon}^{E} P(\varepsilon|E)T(E)\,\mathrm{d}E \\ &= \int_{\varepsilon}^{E} P^0(\varepsilon|E)\exp[-\lambda_0(E) \\ &\quad -\lambda_1(E)\varepsilon^k]T(E)\,\mathrm{d}E \end{aligned} \tag{18}$$

Three photon energies were available: the Ar(II) resonance line at 13.47 eV, the Ne(I) doublet at 16.67–16.85 eV, and the He(I) resonance line at 21.21 eV. Each of them generates its own distribution function $T(E)$, leading to average internal energies of $C_5H_5N^+$ (measured with respect to the dissociation asymptote) equal to 1.13 eV (for Ar(II)), to 2.22 eV (for Ne(I)) and to 2.76 eV (for He(I)). Note that for the first two wavelengths these values are lower than the isomerization barriers reported in Table 1.

6. Results

6.1. Lagrange parameters and kinetic energy release distributions

Fitting the retarding potential curves to Eq. (9) requires choosing an appropriate trial function for the variation of the Lagrange parameter λ_1 with internal energy E. We tried three functional forms: a constant, a linear function and an exponential function. The Lagrange parameters resulting from the fitting procedure were then inserted into Eq. (13) leading to the corresponding kinetic energy release distributions. Based on our previous experience, we tested two constraints, viz. $\varepsilon^{1/2}$ and ε. The quality of the fits (see Fig. 2), as measured by the χ^2 values, was not significantly different for each of the two constraints, whatever the resonance line used. Probably due to the large internal energy covered by these experiments, we cannot draw any conclusion as to the precise nature of the constraint. Based on our previous study in the metastable range [28], which unambiguously identified $\varepsilon^{1/2}$ as the appropriate constraint, we shall mainly show data obtained with this constraint. The important physical observables, i.e., the average kinetic energy release or the ergodicity index, are however, only slightly dependent on the choice of the constraint (see Section 6.3).

The KERDs resulting from the fits are an average over the corresponding internal energy distributions, $T(E)$. It is, therefore, not surprising that the values of the Lagrange parameters will be most reliable at energies where the internal energy distribution is

larger. In keeping with this argument, the Lagrange parameters resulting from the three kinds of energy dependence investigated (constant, linear or exponential) are found to overlap in an energy domain close to the average internal energy. We trust that these values of λ_1 are particularly robust, so that, in the discussion, we will only mention, for each kind of experimental condition, the results obtained in the energy region where the three trial functions overlap. By using three different resonance lines (He(I), Ne(I) and Ar(II)), we sample different energy regions, and are therefore, able to observe the evolution of the reaction dynamics as a function of internal energy. For the three resonance lines, Fig. 3 shows the kinetic energy release distributions $P(\varepsilon|E)$ obtained with this particularly reliable value of λ_1 and the corresponding prior distributions $P^0(\varepsilon|E)$. It is straightforward from this figure that the experimental KERDs are substantially narrower than the corresponding prior ones. This indicates that the dynamical constraint plays an essential role that will be discussed in Section 7.1.

6.2. Average translational energy release

The average kinetic energy release has been evaluated using Eq. (19) at the energies at which a reliable value of λ_1 could be obtained, as explained in Section 6.1:

$$\langle\varepsilon\rangle(E) = \int_0^E \varepsilon P(\varepsilon|E)\,\mathrm{d}\varepsilon \tag{19}$$

The results are plotted in Fig. 4 for both constraints $\varepsilon^{1/2}$ or ε. The average released translational energy $\langle\varepsilon\rangle(E)$ calculated from the two possible constraints shows the same evolution as a function of the internal energy E.

The function $\langle\varepsilon\rangle(E)$ can also be calculated for the prior distribution. This information is also included in Fig. 4 which then compares the actual average release with that to be expected if the reaction proceeded in a totally ergodic way. This comparison reveals clearly that phase space sampling for reaction (1) is incomplete. Furthermore, as already deduced from Fig. 3, it also clearly shows that the effect of the constraint is to discriminate against large translational energy releases. This result is in agreement with our previous studies [13–15,28], and will be discussed in Section 7.

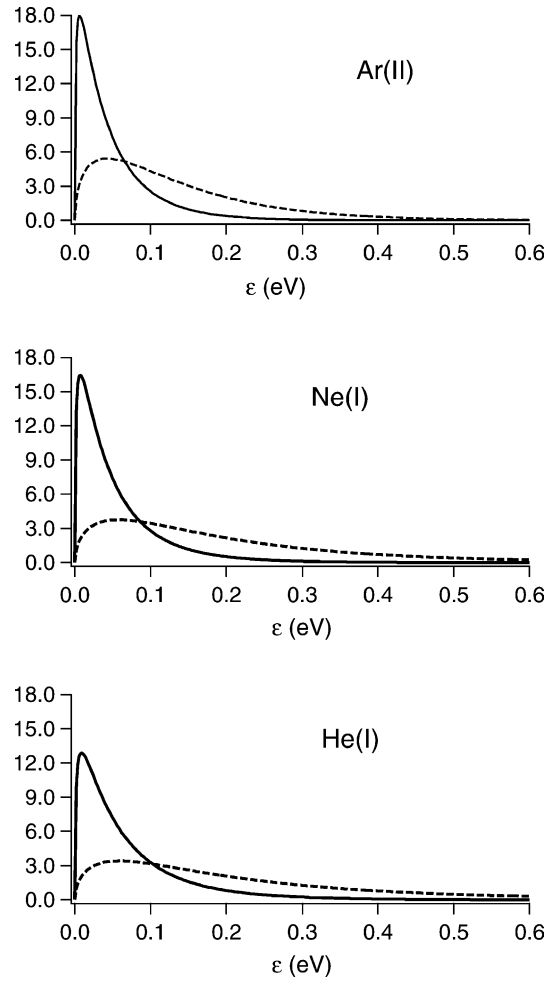

Fig. 3. Kinetic energy release distributions for the reaction $C_5H_5N^+ \rightarrow C_4H_4^+ + HCN$. Solid line: $P(\varepsilon|E)$ calculated at the internal energy E where the $\lambda_1(E)$ value is particularly reliable (see text). Top: $E = 1.1$ eV for Ar(II); middle: $E = 2.6$ eV for Ne(I); bottom: $E = 3$ eV for He(I). Dashed line: $P^0(\varepsilon|E)$ at the same internal energies. The constraint is assumed to be $\varepsilon^{1/2}$.

6.3. Evolution of the ergodicity index with internal energy

The Lagrange parameters $\lambda_0(E)$ and $\lambda_1(E)$ obtained in the first step of the maximum entropy analysis

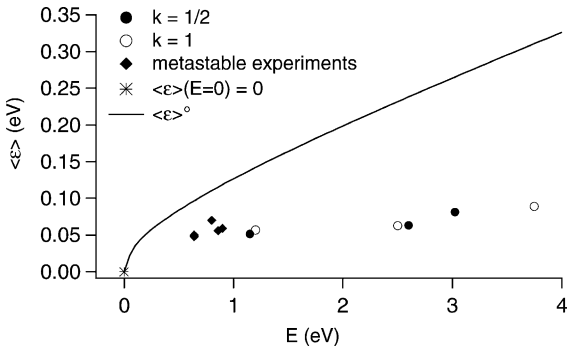

Fig. 4. Averaged kinetic energy release $\langle\varepsilon\rangle(E)$. The circles correspond to the present measurements. The full circles are derived from an assumed constraint $\varepsilon^k = \sqrt{\varepsilon}$ and the empty circles from $\varepsilon^k = \varepsilon$. The diamonds are relative to the metastable experiments [28]. The star in ($E = 0$, $\langle\varepsilon\rangle = 0$) means that exactly at the dissociation threshold, there is no translational energy release. The solid line stands for $\langle\varepsilon\rangle^0$, i.e., the averaged kinetic energy release for the prior distribution $P^0(\varepsilon|E)$.

(Section 6.1) can be inserted into Eq. (15) to find the entropy deficiency, DS(E), and the associated ergodicity index, $F(E)$, that is displayed in Fig. 5 for both isotopomers. At threshold ($E = 0$), the phase space reduces to one single cell. Then the system necessarily occupies 100% of its available phase space. Note that the data obtained in the metastable window [28] fit in very well with the present results. In line with previous studies [15,43], an initial decrease of the ergodicity index from the statistical situation at threshold is followed by a leveling-off at internal energies higher than 2.5 eV. It is, however, not possible to decide from the data whether F will increase again at higher energies. Fig. 5 shows also that the impact of perdeuteration on phase space sampling is not easily assessed. At least at high energy, the exploration of phase space seems to be slightly better for the deuterated ion.

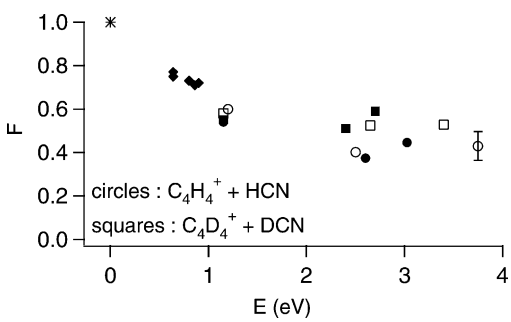

Fig. 5. Ergodicity index F as a function of internal energy E. The circles correspond to the present measurements on undeuterated pyridine $C_5H_5N^+$, the squares correspond to the present measurements on deuterated pyridine $C_5D_5N^+$. The full symbols stand for the constraint $\varepsilon^k = \sqrt{\varepsilon}$ and the empty symbols for $\varepsilon^k = \varepsilon$. The diamonds are derived from the metastable experiments [28]. The star indicates a fully statistical situation at threshold. An error bar gives an estimate of the measurement uncertainties.

7. Discussion

7.1. Phase space sampling

The dissociation of the pyridine ion in the metastable range, corresponding to internal energies of the order of 0.6–0.9 eV above the dissociation threshold, has been previously studied by the MIKES technique [28]. In this low-energy range, the appropriate value of the exponent k to be used in Eq. (13) is found to be equal to 0.5. In other words, a single constraint, unambiguously identified as $\varepsilon^{1/2}$ (i.e., representing the linear momentum) suffices to account for the experimentally observed KERD.

This observation has been rationalized in terms of the "momentum gap law" [14,28]. Most unimolecular reactions can be described as vibrational predissociations [1,44]. In quantum–mechanical terms, the predissociation rate constant (i.e., the transition probability) is determined by the magnitude of the square modulus of the off-diagonal matrix element $\langle n|\hat{V}|\varepsilon\rangle$, where $|n\rangle$ represents the stable state, $|\varepsilon\rangle$ is the unbound state, and $\hat{V}$ is the interaction operator. The higher the translational momentum, the more rapidly the wave function of the unbound state $|\varepsilon\rangle$ oscillates along the reaction coordinate, the smaller the overlap $\langle n|\varepsilon\rangle$ and the matrix element $\langle n|\hat{V}|\varepsilon\rangle$, and finally, the less probable the transition. This observation is termed the "momentum gap law" and the constraint is then associated with a value $k = 1/2$ [14,28]. Its effect is to discriminate against states characterized by a large translational momentum, and therefore, against a large kinetic energy release. In other words, the momentum gap law can be

viewed as an extension of the Franck–Condon principle, which says that nuclei are able to change their linear (translational) momentum only reluctantly.

The present experiments sample a much wider range of internal energies than the MIKES measurements. Any change in the nature of the constraint (e.g., $\varepsilon^{1/2}$ at low energies and ε at high energies) might indicate that the reaction mechanism changes as a function of the internal energy or might indicate a kind of transition state switching [45–51]. Therefore, several values of the exponent k in Eqs. (9) and (13) were tried. As mentioned in Section 6.1, values $k = 1/2$ and 1 both led to satisfactory fits to the experimental data. Thus, neither the exact specification of the constraint (i.e., the appropriate value of the coefficient k), nor the function $\lambda_1(E)$ (which depends of course on the choice of k) can be unequivocally determined. However, what determines the relationship between $P(\varepsilon|E)$ and $P^0(\varepsilon|E)$ is the product $\lambda_1(E)\varepsilon^k$. It is gratifying to note that the uncertainty on their product, i.e., on the argument of the exponential appearing in Eq. (13), is less than the individual uncertainties on each factor. For that reason, the entropy deficiencies DS and ergodicity indices $F(E)$ calculated from the two possible constraints $\varepsilon^{1/2}$ or ε do not greatly differ. Therefore, the variation of the ergodicity index as a function of the internal energy, $F(E)$, represented in Fig. 5, is believed to be quite reliable.

Although the efficiency of phase space sampling is found to be lower than 100%, it does not follow that reaction (1) is non-ergodic at high internal energies. An important distinction between *full* phase space sampling and *representative* sampling has to be introduced. Statistical theories can be applied even if the entire phase space is not completely sampled, i.e., even if F is less than 100%. What matters is the representativity of the sampling on the time scale of the dissociation.

Research based on the theory of autocorrelation functions applied to dissociating systems has shown that what determines the representativity is the selectivity of the initial preparation process [52]. A non-selective excitation process that initially populates even a moderate fraction of the available phase space gives rise to an apparent statistical behavior. This result has been confirmed by classical trajectory calculations [53]. A more stringent experimental test of non-statistical behavior could only be derived from a highly selective initial excitation, i.e., could be obtained only by methods in which the energy is initially deposited in a very small part of the reactant phase space. This is not the case in the present experiment, for reasons that will be examined presently.

Consider again Fig. 5. In the metastable range (low internal energies), the ergodicity index is found to be of the order of 75%. As the internal energy, E increases, the lifetime decreases. The molecule has less time to sample phase space before dissociating and, understandably enough, the ergodicity index decreases. Nevertheless, $F(E)$ seems to stabilize at internal energies higher than 2.5 eV. A similar behavior has already been observed in two cases: loss of a Br atom from $C_2H_3Br^+$ [15] and loss of I from $C_2H_5I^+$ [43]. In the latter cases, a minimum is reached in the $F(E)$ curve, i.e., the leveling off is followed by an increase in the efficiency of phase space sampling. This unexpected increase or even leveling off is thought to result from the multiplication of initial conditions as the energy increases. In fact, following the excitation, internal energy is originally deposited in the electronic degrees of freedom by a large number of vertical Franck–Condon transitions or by autoionization and then relaxes to vibrational and rotational excitation as a result of a cascade of non-radiative transitions. As the internal energy increases, the density of electronic states increases extremely rapidly, and non-adiabatic transitions between potential energy surfaces become extremely frequent. Potential energy surfaces cross along multidimensional lines denoted seams and each point along the seam can serve as an initial condition for a trajectory. The role played by surface crossings in the mechanism of energy randomization had been conjectured by Rosenstock and Krauss 40 years ago [54].

To summarize, the present experiments involve extensive averaging over both a large energy range, and therefore, over a set of presumably very different lifetimes and, furthermore, over widely scattered initial

conditions. The resulting multiplication of initial conditions increases considerably both the ergodicity index and the representativity of the sampling.

7.2. Isotope effect on phase space sampling

The experiments that have been carried out on the reaction $C_5D_5N^+ \rightarrow C_4D_4^+ + DCN$ detected only a marginal isotope effect on the efficiency of phase space sampling (see Fig. 5).

To analyze the possible existence of an isotope effect on phase space sampling, one has to distinguish between bound and unbound molecules. Consider the former first. In general, both experimental [55,56] and theoretical studies [57,58] have focused on the early stages of intramolecular energy redistribution and often do not go beyond the Fermi golden rule level. The autocorrelation function approach [59–61] is much more relevant for the present case of a dissociation process, where an analysis of the long-time limit is required. This approach makes it possible to evaluate Heller's ratio which is equivalent to the ergodicity index, F. The former is defined [59,60] as $F = N_\infty/N^*$, where N_∞ denotes the number of phase-space cells (i.e., the volume in phase space) that is actually explored in the long-time limit [59–61] and N^* is the volume in phase space that would have been sampled if the dynamics were completely chaotic (i.e., the number of all energetically available phase-space cells consistent with the law of energy conservation alone [62]). It is found that there is no isotope effect on the ratio F for bound systems because both the numerator [61] N_∞ and the denominator [62] N^* are found to be proportional to (suitably averaged) densities of states. Hence, both N_∞ and N^* are individually subject to an isotope effect, but their ratio is not.

Let us now examine the situation where a molecule is excited above its dissociation threshold. The flow in phase space is slower for the deuterated species, but its dissociation lifetime increases, both for adiabatic and for non-adiabatic processes. It is difficult to see to what extent the two effects cancel. The differences in phase space sampling for bound and unbound molecules have been analyzed by Remacle and Levine [52]. Dissociating molecules still in a quasibound state can sample the bound part of their phase space faster than what happens below the dissociation asymptote, because they can randomize their energy via overlap with the dissociation continuum. The physical interpretation is termed healing and can be understood in classical terms as a recrossing of the transition state surface leading to a different region of the bound part of phase space. Remacle and Levine conclude, however, that "while healing can significantly enhance the rate of exploration of phase space, it typically is not enough for representative sampling on the time scale of dissociation." However, as emphasized in Section 7.1, the efficiency of phase space sampling in the long-time limit depends on the degree of delocalization of the initial excitation, which is the same for both isotopomers under our experimental conditions. These arguments support, therefore, the observed lack of any significant isotope effect.

8. Concluding remarks

In conclusion, as shown by many authors, the study of translational energy releases provides important information on the underlying reaction dynamics [1,3,47,63–68].

Figs. 3 and 4 show that the translational energy that is actually released in the dissociation of the pyridine ion is definitely less than what is predicted by the prior distribution, i.e., is less than what is expected from a fully statistical theory. The maximum entropy theory translates this observation into an ergodicity index, represented in Fig. 5. The results of the present and also of previous studies can be summarized as follows:

(1) Just as has been observed in a number of previously studied reactions [13–15,28], phase space is not ergodically explored prior to dissociation. As shown by Remacle and Levine [52], it *never* can be fully explored in a unimolecular reaction. All what can be hoped for is *representative* sampling.
(2) The observation that the translational energy release is less than the statistical prediction is satisfactorily accounted for by the momentum

(constraint $= \varepsilon^{1/2}$) or energy (constraint $= \varepsilon$) gap laws, which have been thoroughly studied in the dissociation of van der Waals clusters [69–72]. This systematic tendency against large kinetic energy release implies that the reaction coordinate cannot be treated on equal footing with the bath of the remaining 3N-7 bound degrees of freedom that make up the transition state.

(3) This being said, our study also shows that the gap law, which involves only the energy stored in the reaction coordinate, is the only correction that is needed to improve the statistical treatment. In other words, there is no reason to doubt that energy flows freely among the 3N-7 bound degrees of freedom, i.e., within the transition state. This provides support for the validity of the statistical approach to unimolecular reactions.

(4) The leveling off of the ergodicity index as the internal energy increases strongly suggests that randomization does not result only from spontaneous IVR (i.e., does not mainly result from the anharmonicity of vibrations) but is a consequence of the multiplication of initial conditions, at least at high internal energies.

(5) What remains unclear is this. An unknown part of the entropy deficiency DS and of the fraction of unexplored phase space $[1 - F(E)]$ results from the constraint of angular momentum conservation. The remaining part of DS can be accounted for by the momentum gap law. Unfortunately, the influence of the conservation of angular momentum can so far be rationalized only when the potential between separating fragments is spherically symmetric, which is definitely not the case for reaction (1). In the future, we hope to be able to sort out these two possible sources of dynamical constraints.

Acknowledgements

This work has been supported by the “Actions de Recherche Concertée (ARC)” (Direction de la Recherche Scientifique—Communauté Française de Belgique), the F.N.R.S. (Belgium) and the University of Liège. BL is indebted to the F.N.R.S. (Belgium) for a research associate position.

References

[1] T. Baer, W.L. Hase, Unimolecular Reaction Dynamics: Theory and Experiments, Oxford University Press, New York, 1996.
[2] R.G. Gilbert, S.C. Smith, Theory of Unimolecular and Recombination Reactions, Blackwell, Oxford, UK, 1990.
[3] C. Lifshitz, J. Phys. Chem. 87 (1983) 2304.
[4] J.C. Lorquet, Mass Spectrom. Rev. 13 (1994) 233.
[5] G. Depke, C. Lifshitz, H. Schwarz, E. Tzidony, Angew. Chem. Int. Ed. Engl. 20 (1981) 792.
[6] M. Aschi, J.N. Harvey, C.A. Schalley, D. Schröder, H. Schwarz, Chem. Commun. (1998) 531.
[7] J.N. Harvey, M. Aschi, H. Schwarz, W. Koch, Theor. Chem. Acc. 99 (1998) 95.
[8] J.N. Harvey, M. Aschi, Phys. Chem. Chem. Phys. 1 (1999) 5555.
[9] R.D. Levine, R.B. Bernstein, in: W.H. Miller (Ed.), Dynamics of Molecular Collisions, Part B, Plenum Press, New York, 1976, p. 323.
[10] R.D. Levine, J.L. Kinsey, in: R.B. Bernstein (Ed.), Atom–Molecule Collision Theory. A Guide for the Experimentalist, Plenum Press, New York, 1979.
[11] R.D. Levine, Adv. Chem. Phys. 47 (1981) 239.
[12] R.D. Levine, R.B. Bernstein, Molecular Reaction Dynamics and Chemical Reactivity, Oxford University, New York, 1987.
[13] P. Urbain, F. Remacle, B. Leyh, J.C. Lorquet, J. Phys. Chem. 100 (1996) 8003.
[14] P. Urbain, B. Leyh, F. Remacle, A.J. Lorquet, R. Flammang, J.C. Lorquet, J. Chem. Phys. 110 (1999) 2911.
[15] A. Hoxha, R. Locht, A.J. Lorquet, J.C. Lorquet, B. Leyh, J. Chem. Phys. 111 (1999) 9259.
[16] J.H. Eland, J. Berkowitz, H. Schulte, R. Frey, Int. J. Mass Spectrom. Ion Phys. 28 (1978) 297.
[17] P.C. Burgers, J.L. Holmes, Int. J. Mass Spectrom. Ion Process. 58 (1984) 15.
[18] C. Lifshitz, J. Phys. Chem. 86 (1982) 606.
[19] H.M. Rosenstock, R. Stockbauer, A.C. Parr, Int. J. Mass Spectrom. Ion Phys. 38 (1981) 323.
[20] T. Baer, G.D. Willet, D. Smith, J.S. Phillips, J. Chem. Phys. 70 (1979) 4076.
[21] C. Lifshitz, D. Gibson, K. Levsen, I. Dotan, Int. J. Mass Spectrom. Ion Phys. 40 (1981) 157.
[22] P. Ausloos, J. Am. Chem. Soc. 103 (1981) 3931.
[23] R. Arakawa, M. Arimura, Y. Yoshikawa, Int. J. Mass Spectrom. Ion Process. 64 (1985) 227.
[24] S.W. Staley, T.D. Norden, J. Am. Chem. Soc. 111 (1989) 445.
[25] V. Hrouda, M. Roeselova, T. Bally, J. Phys. Chem. A 101 (1997) 3925.
[26] W.J. van der Hart, Int. J. Mass Spectrom. Ion Process. 176 (1998) 23.

[27] G. Koster, W.J. van der Hart, Int. J. Mass Spectrom. Ion Process. 163 (1997) 169.
[28] P. Urbain, B. Leyh, F. Remacle, J.C. Lorquet, Int. J. Mass Spectrom. Ion Process. 185/186/187 (1999) 155.
[29] R. Locht, Int. J. Mass Spectrom. Ion Process. 148 (1995) L17.
[30] C. Servais, R. Locht, Chem. Phys. Lett. 236 (1995) 96.
[31] A. Hoxha, B. Leyh, R. Locht, Rapid Commun. Mass Spectrom. 13 (1999) 275.
[32] Y. Alhassid, R.D. Levine, J. Chem. Phys. 67 (1977) 4321.
[33] F. Iachello, R.D. Levine, Europhys. Lett. 4 (1987) 389.
[34] P.C. Burgers, J.L. Holmes, A. Mommers, J.K. Terlouw, Chem. Phys. Lett. 102 (1983) 1.
[35] P.C. Burgers, J.L. Holmes, A.A. Mommers, J.E. Szulejko, J.K. Terlouw, Org. Mass Spectrom. 19 (1984) 442.
[36] C. Wesdemiotis, F.W. McLafferty, Chem. Rev. 87(1987) 485.
[37] M.-Y. Zhang, C. Wesdemiotis, M. Marchetti, P.O. Danis, J.J.C. Ray, B.K. Carpenter, F.W. McLafferty, J. Am. Chem. Soc. 111 (1989) 8341.
[38] M.-Y. Zhang, B.K. Carpenter, F.W. McLafferty, J. Am. Chem. Soc. 113 (1991) 9499.
[39] B.J. Shay, M.N. Eberlin, R.G. Cooks, J. Am. Soc. Mass Spectrom. 3 (1992) 518.
[40] G. Koster, W.J. van der Hart, Int. J. Mass Spectrom. Ion Process. 163 (1997) 81.
[41] F. Jensen, Introduction to Computational Chemistry, Wiley, Chichester, 1999.
[42] A.P. Scott, L. Radom, J. Phys. Chem. 100 (1996) 16502.
[43] J.C. Lorquet, J. Phys. Chem. A 104 (2000) 5422.
[44] G. Herzberg, Molecular Spectra and Molecular Structure. III. Electronic Spectra and Electronic Structure of Polyatomic Molecules, Van Nostrand, Princeton, NJ, 1967.
[45] M.T. Bowers, M.F. Jarrold, W. Wagner-Redeker, P.R. Kemper, L.M. Bass, Faraday Discuss. Chem. Soc. 75 (1983) 57.
[46] W.J. Chesnavich, L. Bass, T. Su, M.T. Bowers, J. Chem. Phys. 74 (1981) 2228.
[47] W.J. Chesnavich, M.T. Bowers, Prog. React. Kinet. 11 (1982) 137.
[48] C. Lifshitz, Adv. Mass Spectrom. 11A (1989) 713.
[49] C. Lifshitz, Adv. Mass Spectrom. 12 (1992) 315.
[50] D.G. Truhlar, W.L. Hase, J.T. Hynes, J. Phys. Chem. 87 (1983) 2664.
[51] D.G. Truhlar, B.C. Garrett, S.J. Klippenstein, J. Phys. Chem. 100 (1996) 12771.
[52] F. Remacle, R.D. Levine, J. Phys. Chem. 95 (1991) 7124.
[53] H.W. Schranz, L.M. Raff, D.L. Thompson, J. Chem. Phys. 95 (1991) 106.
[54] H.M. Rosenstock, M. Krauss, Adv. Mass Spectrom. 2 (1963) 251.
[55] J.E. Gambogi, R.P. L'Esperance, K.K. Lehmann, B.H. Pate, G. Scoles, J. Chem. Phys. 98 (1993) 1116.
[56] D.B. Moss, C.S. Parmenter, J. Chem. Phys. 98 (1993) 6897.
[57] T. Uzer, Phys. Rep. 199 (1991) 73.
[58] M. Gruebele, Adv. Chem. Phys. 114 (2000) 193.
[59] E.J. Heller, Phys. Rev. A 35 (1987) 1360.
[60] J.C. Lorquet, V.B. Pavlov-Verevkin, J. Chem. Phys. 93 (1990) 520.
[61] V.B. Pavlov-Verevkin, J.C. Lorquet, J. Phys. Chem. A 106 (2002) 6694.
[62] V.B. Pavlov-Verevkin, J.C. Lorquet, J. Chem. Phys. 104 (1996) 1362.
[63] T. Baer, Adv. Chem. Phys. 64 (1986) 111.
[64] I. Powis, Acc. Chem. Res. 20 (1987) 179.
[65] Z. Szilagyi, K. Vekey, Eur. Mass Spectrom. 1 (1995) 507.
[66] E. Uggerud, Mass Spectrom. Rev. 18 (1999) 285.
[67] J.H. Moon, J.C. Choe, M.S. Kim, J. Phys. Chem. A 104 (2000) 458.
[68] J. Laskin, C. Lifshitz, J. Mass Spectrom. 36 (2001) 459.
[69] J.A. Beswick, J. Jortner, Adv. Chem. Phys. 47 (1981) 363.
[70] G.E. Ewing, J. Chem. Phys. 71 (1979) 3143.
[71] G.E. Ewing, J. Chem. Phys. 72 (1980) 2096.
[72] M.I. Lester, Adv. Chem. Phys. 96 (1996) 51.